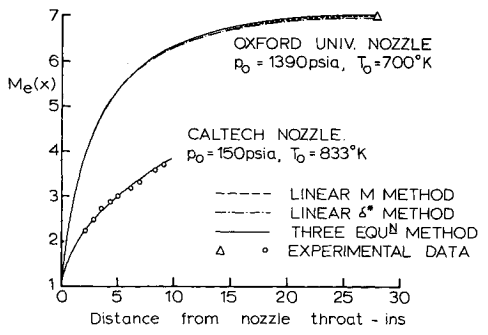

Fig. 1 Comparison of calculated and experimental nozzle Mach numbers.

numbers[3] are shown for comparison. The difference between the experimental and the theoretical results within the nozzle can be attributed to the fact that the measured value is the Mach number at the edge of the boundary layer, whereas because of the use of Eqs. (9, 10 and 12), the theories predict an average value of the Mach number at a cross section. In practice in an expanding supersonic flow $M_e(x) \gtrsim M_e$, as shown by the results. The exit values of the Mach number are in good agreement. Also in Fig. 1 are shown the calculated and experimental Mach numbers for the Oxford University Mach 7 contoured nozzle.[4] Again the differences between the three methods are negligible. It is interesting to note that the values of the exit Mach number predicted by the three equations method for both the nozzles are in close agreement with the experimental values.

Figure 2 shows the variation of the Mach number and boundary-layer characteristics at the exit of the contoured nozzle with the wall to stagnation enthalpy ratio and the freestream unit Reynolds number. These calculations were made with the three equations method. It is seen that the Mach number and boundary-layer characteristics change significantly with changes in the wall temperature and total pressure, contrary to practice in which it is often assumed that the exit Mach number, and hence δ^*, remains constant with changes in driver conditions. Comparison of the predicted and experimental values of C_f and θ have not been made due to a lack of experimental data.

Conclusions

1) The three methods proposed for calculations of the compressible turbulent boundary layer in supersonic nozzles are in close agreement with each other and the experimental results for exit Mach number and displacement thickness. 2) The appreciable variations in the boundary-layer characteristics of nozzles with inlet total pressure and nozzle wall temperature can be readily predicted by the three equations method.

References

[1] Sasman, P. K. and Cresci, R. J., "Compressible Turbulent Boundary Layer with Pressure Gradient and Heat Transfer," *AIAA Journal*, Vol. 4, No. 1, Jan. 1966, pp. 19–25.

[2] Bergstrom, E. R. and Raghunathan, S., "Calculations of the Compressible Turbulent Boundary Layer with Pressure Gradient and Heat Transfer in Internal Flows with Particular Reference to Supersonic Nozzles," TT7104, June 1971, Loughborough University of Technology, England.

[3] Back, L. H. and Cuffel, R. F., "Relationship Between Temperature and Velocity Profiles in a Turbulent Boundary Layer Along a Supersonic Nozzle with Heat Transfer," *AIAA Journal*, Vol. 8, No. 11, Nov. 1970, pp. 2066–2069.

[4] Lagraff, J. E., "Comparative Transition Measurements on a Hollow Cylinder Model," ARC 31233, Hyp. 755, Aeronautical Research Council, England.

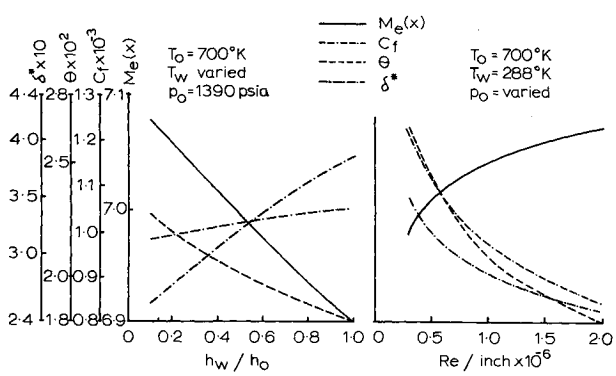

Fig. 2 Variation in nozzle flow parameters with enthalpy ratio and unit Reynolds number.

Binary Diffusion of a Jet Embedded in a Boundary Layer

F. D. HAINS* AND A. J. BAKER†
Bell Aerospace Division of Textron, Buffalo, N.Y.

In some recent studies[1–3] of the penetration and mixing of a hydrogen jet injected normal to a supersonic airstream, the jet turns and remains within the boundary layer. Because of the shape of the boundary-layer velocity profile, the curves of constant concentration form a "Mexican hat" shape as shown in Fig. 1. In this Note, a theoretical model based on the binary diffusion equation is presented along with numerical solution of the governing equation by the method of finite elements.

The dimensionless form of the binary diffusion equation for species A is[4]

$$\vec{V} \cdot \nabla \omega_A = D[\nabla^2 \omega_A + \rho^{-1}(\nabla \rho \cdot \nabla \omega_A)] \tag{1}$$

where ρ is the mixture density, $\vec{V}$ is the fluid velocity, and ω_A is the mass fraction of species A. The diffusivity D is assumed to be constant in Eq. (1). All dimensionless quantities are referenced with respect to the freestream conditions at the first station in x and the characteristic length is chosen so that calculations begin at $x = 1$.

The mixture density is assumed to satisfy the perfect gas law in the dimensionless form

$$\rho = GM/M_B \tag{2}$$

where $G = p/T$. The quantities p and T are the dimensionless pressure and temperature, respectively, and M and M_B are the

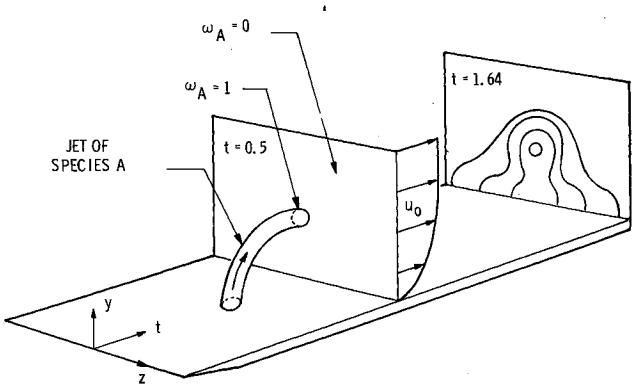

Fig. 1 Diffusion of a jet embedded in a boundary layer.

Received December 6, 1971.

* Principal Scientist, Advanced Technology Research.
† Principal Scientist, Continuum Mechanics Research. Associate Member AIAA.

molecular weights of the mixture and species B, respectively. In general, G will be a function of both x and y.

Substitution of the expression for the molecular weight ratio[4] into Eq. (2) leads to

$$\rho = G[K\omega_A + 1]^{-1} \tag{3}$$

where $K = (M_B - M_A)/M_A$. If $K = 0$, so that the molecular weights of the two species are equal, Eq. (1) is linear. Otherwise, the equation will be nonlinear because of a term of the form $[\nabla\omega_A \cdot \nabla\omega_A]$. This problem can be overcome by introduction of a new variable defined by the transformation

$$\omega_A = (e^{\phi} - 1)/K \tag{4}$$

so that

$$\rho = Ge^{-\phi} \tag{5}$$

Equation (1) is then transformed into the linear equation

$$\vec{V} \cdot \nabla\phi = D[\nabla^2\phi + G^{-1}(\nabla G \cdot \nabla\phi)] \tag{6}$$

In the subsequent analysis, the effects of changes in mixture density on the pressure, velocity and temperature fields are neglected, This is equivalent to decoupling the momentum and energy equations from the binary diffusion equation. The quantities G and $\vec{V}$ in Eq. (6) are obtained from the solution of the boundary-layer equations without diffusion. The first order effects of diffusion are then found from Eq. (6).

The method is illustrated by calculation of the diffusion of a jet embedded in an incompressible flat plate boundary layer. The flow is assumed to be isothermal ($G = 1$), and the two species have identical molecular weights ($K = 0$). The jet core of species A and the surrounding fluid have a velocity distribution given by the momentum integral velocity profile

$$u = (2ct^{-1/2})y - (2c^3t^{-3/2})y^3 + (c^4t^{-2})y^4 \tag{7}$$

where $t = xD$ and $c = 0.2[DRe]^{-0.5}$. The quantity Re is the Reynolds number.

If the velocity components in the y and z directions are neglected in comparison to u, and $(\omega_A)_{tt}$ is neglected in comparison to $(\omega_A)_{yy}$ and $(\omega_A)_{zz}$, Eq. (1) reduces to the diffusion equation

$$u(\omega_A)_t = (\omega_A)_{yy} + (\omega_A)_{zz} \tag{8}$$

The boundary conditions are

$$\left.\begin{aligned} y = 0 &: (\omega_A)_y = 0 \qquad y = \infty : \omega_A = 0 \\ z = 0 &: (\omega_A)_z = 0 \qquad z = \infty : \omega_A = 0 \end{aligned}\right\} \tag{9}$$

For initial conditions, we prescribe a jet of elliptical cross-section located within the boundary layer as shown in Fig. 2. The concentration in the jet is $\omega_A = 1$, and in the surrounding fluid $\omega_A = 0$.

The differential system given by Eqs. (8) and (9) is an elliptic boundary value problem in the transverse plane with parabolic coupling, through the first order convection derivative, to the longitudinal direction. An operational finite element computer

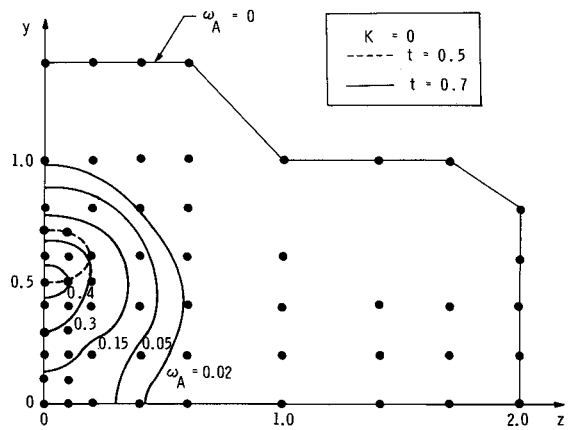

Fig. 2 Mass-fraction concentration lines in the y, z half plane ($t = 0.7$).

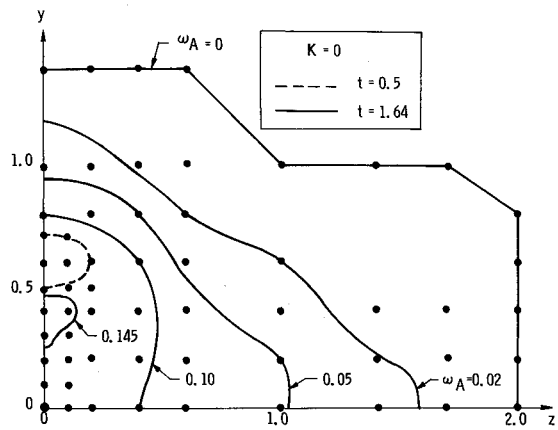

Fig. 3 Mass-fraction concentration lines in the y, z half plane ($t = 1.64$).

program based on the work of Baker[5,6,7] was adapted for solution of this equation.

In this approach, a modal approximation is made to both the main stream velocity u and the mass fraction ω_A. These approximations are valid over triangular shaped subregions R_m of the transverse plane solution domain R and are of the form

$$q_m^*(t, y, z) = \{1, y, z\}\,[\Gamma]_m\,\{Q(t)\}_m \tag{10}$$

where q_m^* is any dependent variable, and the curly brackets denote a column matrix. The square matrix $[\Gamma]_m$ contains elements of known magnitude which transform the polynomial approximation to q_m^* to a representation involving the value of the dependent variable at the fixed vertices of the triangular shaped subregions called nodes. The unknown elements of the vectors $\{Q(t)\}_m$ are the values of the dependent variable at these nodes, and are a function of position along the longitudinal axis. Hence, solution for q_m^* in each finite element is transformed to solution of the elements of $\{Q(t)\}_m$.

Assembly of the solution algorithm is based upon the Method of Weighted Residuals,[8] wherein Eq. (8) is transformed into a much larger system of ordinary differential equations written on the elements of the vector $\{Q(x)\}$, which is the global node distribution of the discretized dependent variable. Solution of this system was obtained from a multiple-predictor-corrector finite difference integration algorithm developed by Nigro.[9]

The finite element solution algorithm has several distinct advantages over conventional finite difference methods. No constraint exists on uniformity of the computational mesh, so that small finite elements can be used where anticipated mass fraction gradients are large, while considerably larger elements can be used in the remaining transverse solution domain. The closure of the solution domain need not coincide with coordinate surfaces, yet arbitrarily mixed combinations of fixed and/or normal gradient boundary conditions on the dependent variable can be routinely accommodated. The method can also accept any specified distribution of material properties based either on tabular input or a relation indicating functional dependence with either the independent or dependent variables.

The node distribution selected for this study is illustrated in Fig. 2. Only half of the $y-z$ plane is considered because $z = 0$ is a plane of symmetry. The boundary conditions at infinity given by Eq. (9) were applied at the irregular shaped boundary in Fig. 2. The nodes are connected by straight lines (not shown, for clarity) to form triangular finite elements. The present discretization employs about 90 finite elements which are made up of 59 nodes. Enforcement of the boundary conditions given by Eq. (9) reduces the number of nodes carried during the integration to 49. Execution of the program for a typical case required about two minutes of central processor time on the IBM 360/65 computer.

The contour lines of constant mass-fraction concentration are shown for two stations in t in Figs. 2 and 3. The initial jet at

$t = 0.5$ indicated by the dashed curve, is shown for comparison. Inside the initial jet, $\omega_A = 1$ and outside of the jet $\omega_A = 0$. Figure 2 shows how the diffusion toward the wall is greater. This is caused by the velocity profile of the boundary layer. For $t = 0.7$ the maximum concentration has dropped to 0.4 and the location of the maximum contour has drifted toward the wall. Two of the smaller concentration lines end on the wall surface.

When $t = 1.64$, as shown in Fig. 3, the maximum concentration drops to 0.145 and the contour line has moved closer to the wall. Near the wall where the velocities are small, a fluid element has more time to diffuse as it moves between the stations given in Figs. 2 and 3. As a result, there is a greater lateral movement of the concentration lines in the vicinity of the wall.

The contour shapes shown here are similar to those measured in the supersonic mixing experiments described in Refs. 1–3. However, in high-speed flows, the compressibility and vorticity diffusion effects which were neglected in the present analysis may be important. In those cases where these effects are small, the present method may yield useful results.

References

[1] Henry, J. R., "Recent Research on Fuel Injection and Mixing and Piloted-Ignition for Scramjet Combustors," *Twelfth Symposium on Combustion*, The Combustion Inst., Pittsburgh, 1969, pp. 1175–1182.

[2] Torrence, M. G., "Concentration Measurements of an Injected Gas in a Supersonic Stream," TN D-3860, April 1967, NASA.

[3] Rogers, R. C., "The Penetration and Mixing of a Sonic Hydrogen Jet Injected Normal to a Mach 4 Airstream," M.S. thesis, March 1970, Virginia Polytechnic Inst., Blacksburg, Va.

[4] Bird, R. B., Stewart, W. E., and Lightfoot, E. N., *Transport Phenomena*, John Wiley & Sons, New York, 1960, p. 557.

[5] Baker, A. J., "A Numerical Solution Technique for a Class of Problems in Fluid Dynamics, Formulated with the Use of Discrete Elements," TCTN-1005, 1969, Bell Aerosystems, Buffalo, N.Y.

[6] Baker, A. J., "Numerical Solution to the Dynamics of Viscous Fluid Flow by a Finite-Element Algorithm; A First Step Towards Computational Continuum Mechanics," *Proceedings of the International Association for Shell Structures Pacific Symposium*. Univ. of Hawaii, Oct. 1971.

[7] Baker, A. J., "A Finite-Element Computational Theory for the Mechanics and Thermodynamics of a Viscous, Compressible, Multi-Specie Fluid," Rept. 9500–920200, 1971, Bell Aerospace, Buffalo, N.Y.

[8] Finlayson, B. A. and Scriven, L. E., "The Method of Weighted Residuals—A Review," *Applied Mechanics Review*, Vol. 19, No. 9, 1966, pp. 735–748.

[9] Nigro, B. J., "The Derivation of Optimally Stable, K-Stage, One-Step, Explicit Numerical Integration Methods," TCTN-1008, 1970, Bell Aerospace, Buffalo, N.Y.

Pressure Distribution on a Yawed Wedge Interacted by an Oblique Shock

M. G. CHOPRA*

Defence Science Laboratory, Delhi, India

AN analytical method developed by Lighthill[1,2] for plane normal shock and later extended for oblique shocks by Srivastava[3] and Srivastava and Chopra[4] has now been applied to the diffraction of oblique shocks advancing over yawed wedges for the case when the relative flow behind the reflected shock is subsonic. Computations have also been undertaken to explore the pressure distribution on the wedge surface.

Received December 14, 1971; revision received February 1, 1972. The author is thankful to M. J. Lighthill, and R. R. Aggarwal for their interest in the work; R. S. Srivastava for his guidance, and Director Defence Science Laboratory for allowing its publication.

Index categories: Shock Waves and Detonations; Supersonic and Hypersonic Flow; Nonsteady Aerodynamics.

* Senior Scientific Officer.

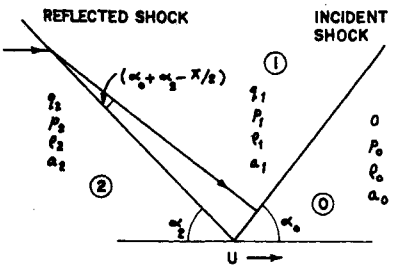

Fig. 1 Oblique shock configuration.

As the oblique shock configuration (Fig. 1) advances over a yawed wedge (shock line making some nonzero angle with the leading edge of the wedge), the point of intersection of the leading edge and the shock line moves with the velocity $U \csc \chi$, U and χ being the velocity of the shock line and angle of yaw, respectively. The whole configuration can be brought to rest by superimposing a velocity $U \csc \chi$ along the leading edge (Fig. 2) and for ensuring conical flowfield behind the reflected shock the angle of yaw must satisfy the inequality

$$\sin^2 \chi < U^2/(a_2^2 + 2Uq_2 - q_2^2)$$

In fact, the limit on χ depends both on the incident shock strength and the angle of incidence. For a particular shock strength as the angle of incidence increases from the sonic angle to the extreme angle the limiting value of χ decreases and attains its minimum for extreme angle. The limit on χ for different shock strengths taking angle of incidence equal to extreme angle is depicted graphically (Fig. 3) and it is observed that it decreases slowly as the shock strength varies from 0 to 0.6, increases slowly thereafter and finally shows steep rise as the shock strength varies from 0.9 to 1.0. Chester[5] also found out a similar restriction on the angle of yaw but it varied with shock strength only.

Let the perturbations introduced in the flow behind the reflected shock have components u_1, v_1 and w_1 referred to Cartesian coordinate system (x', y', z') such that z' axis is along the axis of the cone of disturbance and x' is perpendicular to z' axis lying in the plane of the wedge and passing through the point of intersection of shock line and leading edge. The flow picture (Fig. 4) obtained in a plane normal to the axis of the Mach cone is the same as for the case of interaction of oblique shock with unyawed wedges (shock line making zero angle with the leading edge) with the only difference that in the problem of interaction of unyawed wedges the flow picture grows with respect to time whereas in the present case it can be regarded to be growing with the axis of the cone of disturbance. In fact, for the unyawed case the cone of disturbance will degenerate into a cylinder, the axis of the cone becoming parallel to the leading edge and the vertex of the cone approaching infinity. With the help of conical field transformations used by Chester,[5] the physical situation may be translated into the following boundary value problem in terms of perturbed pressure p. Differential equation

$$\frac{\partial^2 p}{\partial x^2} + \frac{\partial^2 p}{\partial y^2} = \left(x\frac{\partial}{\partial x} + y\frac{\partial}{\partial y} + 1\right)\left(x\frac{\partial p}{\partial x} + y\frac{\partial p}{\partial y}\right) \qquad (1$$

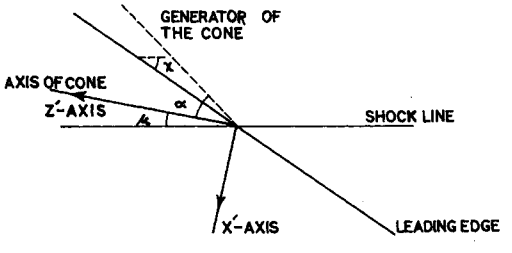

Fig. 2 Configuration after interaction in the x'–z' plane.